ACS APPLIED ELECTRONIC MATERIALS

pubs.acs.org/acsaelm
Article

Dependence of the Metal−Insulator−Semiconductor Schottky Barrier Height on Insulator Composition

Benjamin E. Davis* and Nicholas C. Strandwitz

Cite This: ACS Appl. Electron. Mater. 2024, 6, 770−776
Read Online

ACCESS | Metrics & More | Article Recommendations | Supporting Information

ABSTRACT: The effects of different high-κ tunnel oxides on the metal−insulator−semiconductor Schottky barrier height (Φ_B) were systematically investigated. While these high-κ interlayers have been previously observed to affect Φ_B, there has never been a clear consensus as to why this Φ_B modulation occurs. Changes in Φ_B were measured when adding 0.5 nm of seven different high-κ oxides to n-Si/Ni contacts with a thin native silicon oxide also present. Depending on the high-κ oxide composition and Φ_B measurement technique, increases in Φ_B up to 0.4 eV and decreases up to 0.2 eV with a high-κ introduction were measured. The results were compared to several different hypotheses regarding the effects of tunnel oxides on Φ_B. The experimental data correlated most closely with the model of a dipole formed at the SiO_x/high-κ interface due to the difference in the oxygen areal density between the two oxides. Knowledge of this relationship will aid in the design of Schottky and ohmic contacts by providing criteria to predict the effects of different oxide stacks on Φ_B.

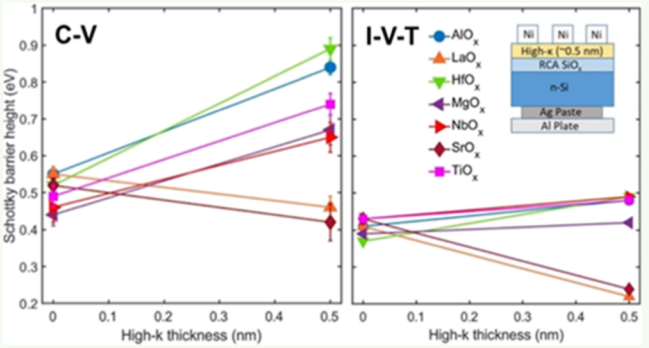

KEYWORDS: *Schottky barriers, atomic layer deposition, tunnel oxides, thin films, interface dipoles*

INTRODUCTION

It is desirable to control the Schottky barrier height (Φ_B) at the metal−semiconductor contacts for a variety of applications. For example, Φ_B minimization is needed for ohmic contacts. Decreasing Φ_B is a key factor in reducing parasitic resistance at transistor source/drain contacts, which is of importance for continued scaling down of device dimensions.[1−3] The formation of a Schottky barrier at electrical contact interfaces also impedes charge carrier collection in certain photovoltaic architectures.[4,5] In other cases, maximization of Φ_B is desirable. In Schottky barrier solar cells, a large Φ_B is necessary to separate photogenerated electron−hole pairs and prevent recombination.[6,7] Power rectifiers utilize a large Φ_B to achieve a high turn-on voltage and reduce leakage current in the "off" state.[8] Variation in interfaces and insulating layers in metal−insulator−semiconductor (MIS) stacks has a dramatic impact on Φ_B but an accurate predictive framework for these systems does not yet exist.

According to the basic Schottky model, the barrier height between a metal and an n-type semiconductor is only a function of the vacuum metal work function $\Phi_{M,vac}$ and the semiconductor electron affinity X_S[9]

$$\Phi_B = \Phi_{M,vac} - X_S \quad (1)$$

In practice, eq 1 rarely agrees with experimental values of Φ_B. Often, the metal work function has little effect on the value of Φ_B. According to the concept of Fermi level pinning

$$\Phi_B = \Phi_{CNL} + S(\Phi_{M,vac} - \Phi_{CNL}) - X_S \quad (2)$$

where Φ_{CNL} is the charge neutrality level in the semiconductor and S is a "pinning" factor that determines the sensitivity of Φ_B to $\Phi_{M,vac}$. Thus, eq 2 utilizes an "effective" metal work function that depends on the pinning factor and the charge neutrality level, instead of solely $\Phi_{M,vac}$.[10]

If an electrostatic dipole moment ($\Delta\Phi_{B,d}$) is also present at the contact, then it is also expected to impact Φ_B

$$\Phi_B = \Phi_{CNL} + S(\Phi_{M,vac} - \Phi_{CNL}) - X_S + \Delta\Phi_{B,d} \quad (3)$$

Insertion of a tunnel active insulating layer between the metal and semiconductor can affect Φ_B through changes in the S factor and interface moment. Several possible reasons for the resulting effect on Φ_B have been discussed in the literature, including the insulator causing "depinning" of the Fermi level (i.e., a higher value of S and greater influence of the metal work function),[11] the electrostatic effect of dielectric fixed charges, and the potential to form electric dipoles at interfaces. Aluminum oxide fixed charges may contribute to changes in

Received: September 6, 2023
Revised: January 3, 2024
Accepted: January 3, 2024
Published: January 18, 2024

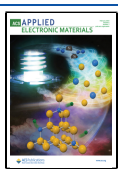

Table 1. ALD Parameters for Growth of Each Oxide

oxide	metal precursor	precursor temp. (°C)	N_2 boost? (Y/N)	O source	reactor temp. (°C)	growth rate (Å/cycle)	number of cycles
AlO_x	trimethylaluminum	~30	N	H_2O	150	0.90	6
HfO_x	tetrakis(dimethylamido) hafnium	75	N	H_2O	150	1.1	5
TiO_x	tetrakis(dimethylamido) titanium	75	N	H_2O	150	0.57	9
MgO_x	bis(ethylcyclopentadienyl) magnesium	90	N	H_2O	150	1.3	4
NbO_x	(*tert*-butylimido)tris(diethylamino) niobium	90	Y	H_2O	150	0.54	9
SrO_x	bis(*n*,*N*′-di-*tert*-butylacetamidinato) strontium(II)dimer	90	Y	O_3	150	0.84	6
LaO_x	tris(*N*,*N*′-di-i-propylformamidinato) lanthanum	160	Y	O_3	200	1.4	4

Φ_B on GaAs substrates.[12] However, experiments have also shown that the alumina fixed charge is not a dominating factor of Φ_B on Si substrates.[13,14] Shifts in the flat band voltage of MIS capacitor structures have been observed when stacking high-κ gate oxides onto interfacial SiO_x, and these shifts are often attributed to dipoles forming at the SiO_x/high-κ interface.[15−17] It was also experimentally demonstrated that such dipoles can be used to tune Φ_B of MIS tunnel structures.[3,13,18]

Several explanations of the origin of the dipoles have been proposed. Kita and Toriumi suggested that dipoles form due to differences in the oxygen areal density (OAD) between two oxides.[19] In this case, bond relaxation would be achieved when negatively charged oxygen ions move from the higher-OAD to the lower-OAD side of the interface, forming Frenkel-type defects and inducing a dipole with a positive charge in the high-OAD side and negative charge in the low-OAD side. This hypothesis is supported by a report on the correlation of XPS-measured electrical dipoles at SiO_x/high-κ interfaces to the XPS-derived oxygen density ratios of the oxides.[20]

Calculations by Lin and Robertson instead indicated that dipoles originate from the parent metal work functions/group electronegativities as long as there was a sufficient difference in the dielectric constant κ between the layers.[21] They argue that dipoles exist along the metal−oxygen bonds on both sides of the oxide interface with dipole strengths related to the parent metal work functions. The relative dielectric constants of the oxide layers then determine to what extent each dipole is "screened" and whether a net dipole will form. Zhu et al. measured SiO_x/high-κ interfacial dipoles via photoelectron spectroscopy and observed that the dipole strength was correlated with the thickness of an interfacial silicate layer between SiO_x and AlO_x.[22]

Several experimental studies have attributed changes in the MIS Φ_B to changes in dipoles formed between insulating layers.[3,13,18,23] However, such electrical experiments on Si have only been performed with a limited selection of high-κ tunnel oxide compositions (namely, AlO_x and LaO_x). An experimental study on a broader selection of oxides provides a platform to test the above hypotheses. Thus, the present study measures the changes in Φ_B upon the introduction of a series of insulator compositions in Si-based MIS structures and compares the results to the hypotheses discussed above.

EXPERIMENTAL SECTION

For diode fabrication (Figure S1), n-type Si substrates with doping density 9×10^{16} cm^{-3} were cleaned with UV−ozone (Jelight) for 5 min and immersed in 5 wt % hydrofluoric acid for 1 min. Immediately after the etch, substrates were sonicated for 5 min in isopropanol (IPA). Finally, substrates were cleaned using the standard RCA process that included sequential immersion in 1:1:5 (by volume) $NH_4OH/H_2O_2/H_2O$ and 1:1:6 $HCl/H_2O_2/H_2O$ solutions for 10 min each at temperatures between 70 and 80 °C.[24] After each wet cleaning step, samples were rinsed with 18.2 MΩ water.

Each sample set contained two control samples with only the terminal RCA SiO_x. Atomic layer deposition (ALD) was used to grow the deposited oxide on other samples using a Cambridge Nanotech Savannah S100 reactor. The deposition parameters for each oxide are shown in Table 1.

After ALD, ~200 nm thick circular Ni top contacts (area = 0.005 cm^2) were deposited by electron-beam evaporation through a shadow mask. Back contacts were made by scratching through the chemical oxide on the back of each sample with a diamond tip, applying Ag paste to the scratched area, and using the paste to fix an Al plate to the sample.

Metal−oxide−semiconductor capacitors (MOSCAPs) were prepared for each deposited high-κ oxide. The MOSCAPs were prepared identically to the diodes except for two details: the samples were etched in HF a second time immediately prior to ALD to minimize interfacial SiO_x, and 10 nm of oxide was deposited instead of 0.5 nm.

Φ_B was measured from diodes using Mott−Schottky (MS) and current−voltage−temperature ($I-V-T$) methods. For MS measurements, capacitance−voltage ($C-V$) data were collected at 1 MHz using a Hewlett-Packard 4194a Impedance/Gain-Phase Analyzer.[25] Φ_B for each condition was averaged over 18 contact pads across two samples. For $I-V-T$ measurements, $I-V$ data were collected at a variety of temperatures using a Keithley 2450 Sourcemeter.[26] The reverse bias current data were used for the fit. $C-V$ measurements were also performed at 1 MHz on the MOSCAPs for the evaluation of κ, the flat-band voltage V_{fb}, and the density of interface states D_{it} via the Terman method for each oxide.[27]

Ten nm high-κ oxide films were measured by X-ray photoelectron spectroscopy (XPS) in a SPECS PHOIBOS 150 NAP-XPS system under ultra-high vacuum to probe the metal oxidation state(s) and oxygen/metal atomic ratio. High-sensitivity low-energy ion scattering was performed with an ION-TOF Qtac100 instrument to investigate substrate coverage after the growth of nominally 0.5 nm of each high-κ film. Finally, the densities of some of the films were measured using X-ray reflectivity in a Panalytical Empyrean diffractometer. Film thicknesses were measured using a J.A. Woollam VASE Spectroscopic Ellipsometer.

In an effort to test trends in Φ_B against the theories discussed above, it was necessary to estimate the OAD of each oxide (Table 2).

Table 2. Parameters Used to Estimate OAD and Obtained Values for Each Oxide

oxide formula	film density (g/cm^3)	density source	OAD (cm^{-2})
Al_2O_3	2.9	various methods[28]	1.48×10^{15}
HfO_2	9.4	XRR[29]	1.42×10^{15}
TiO_2	3.7	XRR[30]	1.45×10^{15}
MgO	3.4 ± 0.2	XRR (in-house)	1.37×10^{15}
Nb_2O_5	3.8 ± 0.4	XRR (in-house)	1.23×10^{15}
SrO	3.1 ± 0.1	XRR (in-house)	6.90×10^{14}
La_2O_3	6.2 ± 0.1	XRR (in-house)	1.07×10^{15}

https://doi.org/10.1021/acsaelm.3c01231
ACS Appl. Electron. Mater. 2024, 6, 770−776

The OAD was estimated by the method described by Kita and Toriumi.[19] This method expresses OAD $\sigma = V_u^{-2/3}$, where V_u is the volume of a unit cell containing a single oxygen atom (e.g., $Al_{2/3}O$ or $Hf_{1/2}O$), equal to the formula weight in grams divided by the film density in g/cm^3. The film density was taken from the literature only when data were available from films synthesized using the same ALD precursors and deposition temperature employed in the present study.

RESULTS AND DISCUSSION

Nonlinear $1/C^2$ vs V curves were observed, so data were corrected by subtracting the "excess capacitance" resulting in more linear $1/C^2$ vs V data and correspondingly nearly constant Φ_B with applied bias (Figure S2).[31] Excess capacitance has been observed as the result of charging and discharging of trap states, and thus may be due to the lack of postdeposition anneal step in this work.[9]

The Φ_B values of the MIS Schottky diodes with native SiO_x or native SiO_x and an additional high-κ oxide were quantified using $C-V$ (Figure 1a) and $I-V-T$ (Figure 1b) techniques.

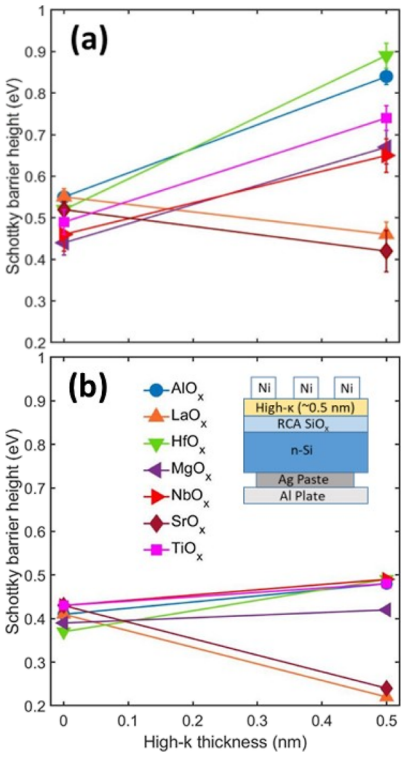

Figure 1. Schottky barrier heights measured via (a) the $C-V$ method and (b) the $I-V-T$ method. The error bars in (a) represent the standard deviations. The inset of (b) is a schematic of the test structure used.

Without a deposited oxide (only native SiO_x), Φ_B values were ~0.5 eV. Some deviation of Φ_B was found among the SiO_x control samples and, hence, the "shifts" in Φ_B within each sample set, rather than the raw values of Φ_B, are considered below. The insertion of a high-κ oxide increased (AlO_x, HfO_x, MgO_x, NbO_x, and TiO_x) or decreased (SrO_x, LaO_x), depending on oxide composition. The magnitudes of the increases with the insertion of the high-κ layer were approximately 0.3−0.4 eV and the magnitude of the decreases was ~0.1 eV for the $C-V$−determined Φ_B. Qualitatively, $I-V-T$-determined trends were the same, but overall Φ_B values were smaller. This behavior is consistent with Φ_B inhomogeneities across the contacts, as measured current is dominated by lower-Φ_B "patches" within the interface, whereas $C-V$ measurements yield the mean Φ_B across the interface area.[32,33] However, the agreement in the trends between the two measurement techniques allows for generalization about the impact of the high-κ composition on Φ_B. Limited data exist in the literature on Φ_B modulation utilizing high-κ layers as thin as those in the present study. However, the $I-V-T$-measured Φ_B increase of 0.1 eV with AlO_x addition is consistent with a corresponding 0.1 eV Φ_B decrease measured on p-type Si in ref 18, which used a similar ALD process to deposit AlO_x onto chemical SiO_x.

Single temperature current density versus voltage ($J-V$) measurements also provide a qualitative assessment of Φ_B (Figure 2). Specifically, if a similar tunnel barrier is presented

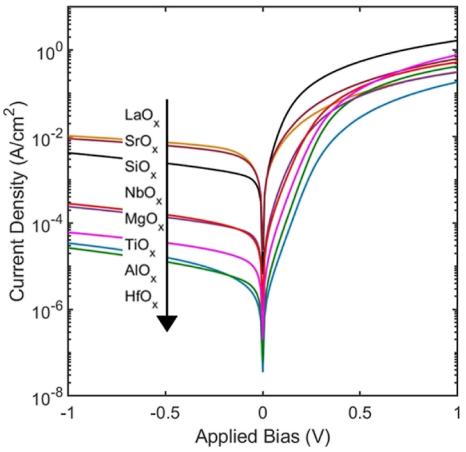

Figure 2. Representative $J-V$ data were collected from diodes with each type of tunnel oxide insulator at room temperature.

to the majority carrier electrons by each oxide layer, and assuming recombination currents are small relative to thermionic emission currents, the reverse saturation current densities (J_{sat}, $V < 0$ V) should be inversely related to Φ_B. Indeed, the LaO_x and SrO_x samples exhibited larger J_{sat} values in reverse bias relative to the SiO_x control sample, and the diodes with the other oxide compositions displayed lower J_{sat} values relative to a representative SiO_x control sample. Further, the diodes with oxides that yielded the largest Φ_B values in MS measurements displayed the lowest J_{sat} values (i.e., AlO_x and HfO_x). Quantitatively, the log of the saturation current density plotted against the $C-V$ and $I-V-T$-derived Φ_B exhibits linear R^2 values of 0.83 and 0.34, respectively (Figure S3). A poor fit is not surprising as the current values are impacted not only by Φ_B but also by the oxide tunnel barrier, which will be affected by oxide composition. However, the qualitative trend provides further evidence of the correct quantification of Φ_B values and trends in these samples. Further, changes in J_{sat} values over 2 orders of magnitude with the same semiconductor substrate and metal composition demonstrate the practical importance of Φ_B control with interfacial layers.

LEIS measurements were used to examine whether full coverage of the Si substrate was achieved by the high-κ oxide depositions or whether films contained exposed SiO_x surfaces (Figure 3). The ALD films were compared with a Si substrate coated in thermally grown SiO_2 that was cleaned with the standard RCA process, treated with atomic oxygen, and sputtered using a 0.5 keV Ar^+ ion beam with a fluence of 1 ×

https://doi.org/10.1021/acsaelm.3c01231
ACS Appl. Electron. Mater. 2024, 6, 770−776

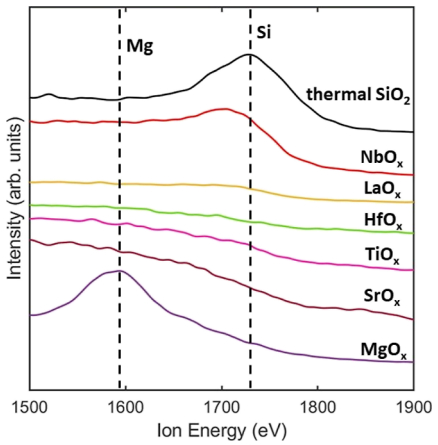

Figure 3. LEIS spectra in the Si energy range from 0.5 nm films of each high-κ oxide and a thermal SiO_2 substrate (top).

10^{15} ions/cm^2. LEIS is highly sensitive to ions scattered by the outermost layer of atoms, in which case a "surface peak" is observed as can be seen for Si and Mg in the thermal SiO_2 and MgO_x samples, respectively. Subsurface scattering from a given element is also observed and will result in ion detection at lower energies than this surface peak.[34] Thus, the absence of a surface peak for Si is expected to be a good qualitative criterion for the total coverage of the SiO_x surface by the high-κ film. AlO_x was not included in these measurements because the Al and Si peaks are too close together to be easily distinguished. The NbO_x spectrum contains a peak between 1700 and 1750 eV, where the Si peak is observed, indicating that some Si surface atoms are exposed and the NbO_x coverage is not complete. None of the other high-κ oxides exhibited a surface peak at these energies, indicating that the surface was completely covered with the deposited high-κ oxide. All oxides exhibited increases in ion yield at ion energies lower than 1800 eV due to subsurface scattering from Si below the deposited oxide surface. Regardless of incomplete coverage, NbO_x had a demonstrable effect on Φ_B and was still considered in the overall trends below.

Several potential factors that may influence Φ_B are compared against the experimental Φ_B data including the parent metal work function, parent metal Pauling electronegativity, measured oxide dielectric constant, and estimated OAD (Figure 4). These comparisons are made based on the $C-V$ data; however, similar results were obtained fitting the qualitatively similar $I-V-T$ data. A weak positive association was found between the observed Φ_B shifts and the known parent metal work functions (R^2 = 0.62, Figure 4a), as well as the parent metal Pauling electronegativities (R^2 = 0.56, Figure 4b).[35] NbO_x was excluded from work function analysis because of the wide range of work functions reported for Nb.[35] No apparent trend was found between the Φ_B shifts and the measured dielectric constants of the ALD oxides (R^2 = 0.09, Figure 4c). However, when comparing the shifts with the estimated OAD values, the strongest correlation is observed among the theories tested (R^2 = 0.81, Figure 4d). Specifically, larger OADs for the high-κ

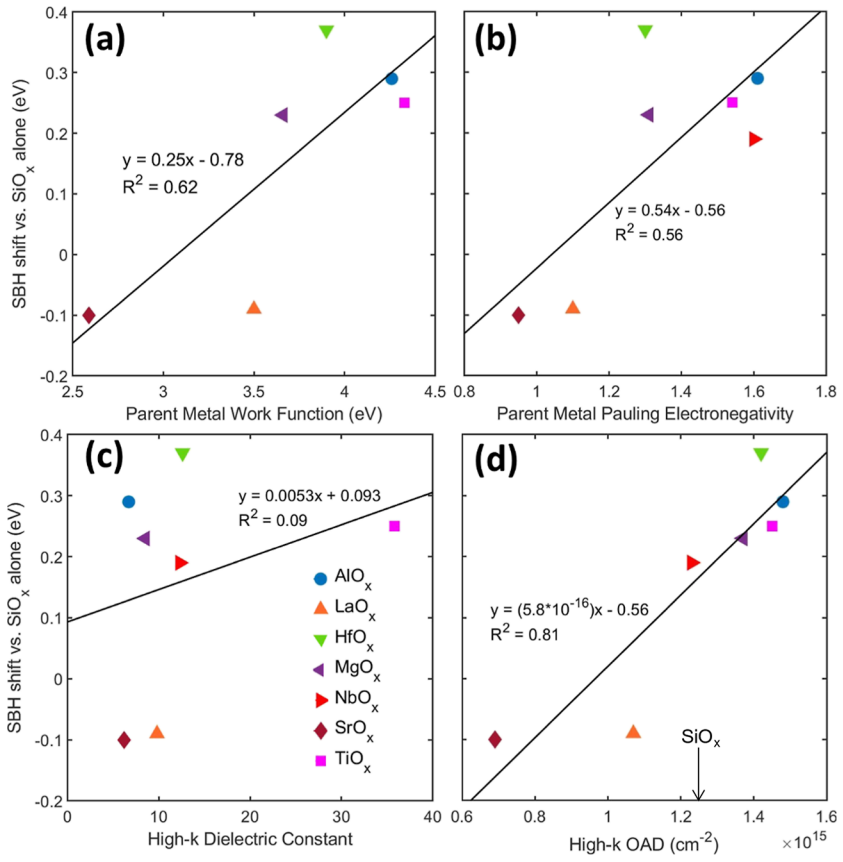

Figure 4. Schottky barrier height shifts quantified from $C-V$ data plotted against the corresponding high-κ oxide's (a) parent metal work function, (b) parent metal Pauling electronegativity, (c) measured dielectric constant, and (d) estimated OAD. The arrow in (d) indicates the approximate OAD of SiO_x, where the Φ_B shift would be expected to be zero.

https://doi.org/10.1021/acsaelm.3c01231
ACS Appl. Electron. Mater. 2024, 6, 770−776

layers resulted in larger Φ_B values. The changes in Φ_B relative to the SiO_x control samples are also consistent with the OAD model. Assuming a stoichiometry of SiO_2 and a film density of 2.2 g/cm^3, the interfacial SiO_2 would have an OAD of approximately 1.2×10^{15} cm^{-2}.[19] All of the films with higher OADs than that of SiO_2 exhibit an increase in Φ_B upon introduction of the high-κ layer, and both of those with a smaller OAD exhibit decrease.

A notable exception to the trend of the OAD versus Φ_B is that the addition of SrO_x and LaO_x induces similar Φ_B shifts despite the significant difference in the estimated OAD between them. Atomic ratios determined by XPS measurements indicated partial conversion of the films to $SrCO_3$ and $La(OH)_3$, whereas the compositions used in the calculations were SrO and La_2O_3. Hence, the OADs estimated for these films may be less accurate than those for the other oxides. A separate plot (not shown) was made for adjusting the formulas in Table 2 based on the atomic ratios measured via XPS. While this approach resulted in a smaller OAD difference between the Sr and La species, it yielded a poorer linear fit overall (R^2 = 0.65). The poor fit is attributed to the difficulty separating contributions in XPS O 1s core level spectra from metal oxides, metal hydroxides, and adventitious contamination, which could lead to erroneous oxygen/metal atomic ratios. Even within a given oxide composition, changes in Φ_B are expected based on thermal processing, native oxide characteristics, and film thickness, such that a perfect correlation of OAD differences and Φ_B are not expected.[3,13,18] LaO_x deposited on Si with the ALD process used in the present study has also been suggested to form an interfacial silicate, and as a result, there may not be a clear SiO_x/high-κ interface with a single dipole.[36,37]

Fermi level depinning was also considered as a possible mechanism for the observed barrier height changes. Assuming a work function of 5.2 eV for Ni, the unpinned Φ_B for n-Si/Ni would be ~1.1 eV.[35] According to the metal-induced gap states (MIGS) theory of Fermi level pinning, the introduction of an interfacial oxide reduces pinning by reducing the overlap between the wave function of electrons in the metal and the semiconductor surface. Such an overlap creates energy states within the semiconductor band gap.[38,39] In this case, it would be expected that Φ_B would increase with the introduction of any high-κ tunnel oxide as it approaches the unpinned value, which was not observed. Thus, while Fermi level depinning in addition to a dipole contribution cannot be ruled out, Fermi level depinning alone is not a likely explanation for the observed results.

Another theory suggests that tunnel oxides passivate intrinsic defect states at the interface to reduce pinning.[40] D_{it} vs surface potential data (Figure S4), calculated from representative $C-V$ data from each MOSCAP, did not display any systematic differences between high-Φ_B oxides (i.e., AlO_x, HfO_x) and low-Φ_B oxides (LaO_x, SrO_x). The AlO_x and SrO_x D_{it}-surface energy curves closely overlapped through most of their ranges. These results suggest that Φ_B modulation is not related to the passivation of the interfacial states.

Φ_B shifts were also plotted against several other parameters, including the parent metal valence, film stoichiometry (i.e., atomic ratios), oxide fixed charge (estimated from measured MOSCAP V_{fb}), and conduction and valence band edge positions below the vacuum level (data not shown). The band edge positions were determined from literature electron affinity and band gap data.[41−52] No correlations were observed in any of these cases. Thus, of the parameters investigated, the estimated OAD provides the most accurate prediction of the change in Φ_B when high-κ oxides are added to a Si/SiO_x/Ni stack. Based on the $C-V$ results, the Φ_B shift when adding a high-κ oxide to the tunnel stack is approximately equal to

$$\Delta\Phi_B = 5.8\cdot10^{-16}(\mathrm{OAD}) - 0.56 \quad (4)$$

OADs also produced the strongest correlation with the $I-V-T$ data with an R^2 value of 0.76, and the linear fit

$$\Delta\Phi_B = 3.9\cdot10^{-16}(\mathrm{OAD}) - 0.50 \quad (5)$$

On other semiconductors, the introduction of tunnel insulators has been shown to result in a similar or identical Φ_B shift when different metal top contacts are used.[39,53] Therefore, it is expected that trends similar to those observed in the present study will apply to other semiconductor/metal systems with an interfacial SiO_x/high-κ oxide tunnel stack.

The data presented support the hypothesis that the effect of high-κ tunnel oxides on Φ_B is dominated by the OAD-induced dipoles, though other effects on Φ_B may exist. The knowledge that the OAD can be used to predict changes in Φ_B will help guide the material choice in the design of future devices. For example, a high-OAD tunnel oxide such as AlO_x or HfO_x can be inserted to maximize Φ_B at a metal/n-Si contact or minimize Φ_B at a metal/p-Si contact. Conversely, a low-OAD oxide such as LaO_x or SrO_x will minimize Φ_B at a metal/n-Si contact or maximize Φ_B at a metal/p-Si contact.

CONCLUSIONS

A systematic study has been conducted on the relationship between high-κ tunnel oxide composition and Φ_B at n-Si/SiO_x/high-κ/Ni contacts to test different hypotheses regarding the source of Φ_B modulation. The changes in Φ_B were measured when adding each of seven different high-κ tunnel oxides to the interface. The results were compared to several different factors proposed to cause the interfacial dipoles that result in V_{fb} or Φ_B changes. The data presented correlate most closely with the model of a dipole at the SiO_x/high-κ interface induced by the difference in the OAD, demonstrating that this is the best available model to predict the effect of such tunnel stacks on Φ_B. The relationship between the oxide OAD and the change it induces in Φ_B was quantified in a linear fit to help guide the design of future devices where control over Φ_B is beneficial, for example, minimizing or eliminating Φ_B for transistor source-drain contacts or maximizing Φ_B for charge carrier separation in photovoltaics and power electronics.[2,7,8]

ASSOCIATED CONTENT

Supporting Information

The Supporting Information is available free of charge at https://pubs.acs.org/doi/10.1021/acsaelm.3c01231.

Process flow diagram illustrating the steps of diode fabrication, representative capacitance−voltage ($C-V$) data and corresponding Mott−Schottky plots corrected for excess capacitance from diodes with each oxide insulator, saturation current density plotted against the $C-V$ and $I-V-T$-derived Schottky barrier height values with linear best-fit lines, and plot of the density of interface states (D_{it}) vs the surface potential calculated from representative MOSCAP $C-V$ data for each high-κ oxide (PDF)

https://doi.org/10.1021/acsaelm.3c01231
ACS Appl. Electron. Mater. 2024, 6, 770−776

AUTHOR INFORMATION

Corresponding Author

Benjamin E. Davis − *Department of Materials Science and Engineering, Lehigh University, Bethlehem, Pennsylvania 18015, United States;* orcid.org/0000-0002-1668-0579; Email: b91.davis@gmail.com

Author

Nicholas C. Strandwitz − *Department of Materials Science and Engineering, Lehigh University, Bethlehem, Pennsylvania 18015, United States*

Complete contact information is available at: https://pubs.acs.org/10.1021/acsaelm.3c01231

Author Contributions

All authors contributed equally to this work.

Funding

This research was funded by NSF grant no. 1605129.

Notes

The authors declare no competing financial interest.

ACKNOWLEDGMENTS

The authors thank Dr. Ryan Thorpe for the collection of XPS data and Md. Istiaque Chowdhury for the collection of XRR data.

REFERENCES

(1) Schroder, D. K.; Meier, D. L. Solar Cell Contact Resistance—A Review. *IEEE Trans. Electron Devices* **1984**, *31* (5), 637−647.

(2) Connelly, D.; Faulkner, C.; Grupp, D. E. Optimizing Schottky S/D Offset for 25-Nm Dual-Gate CMOS Performance. *IEEE Electron Device Lett.* **2003**, *24* (6), 411−413.

(3) Coss, B. E.; Loh, W. Y.; Wallace, R. M.; Kim, J.; Majhi, P.; Jammy, R. Near Band Edge Schottky Barrier Height Modulation Using High- κ Dielectric Dipole Tuning Mechanism. *Appl. Phys. Lett.* **2009**, *95* (22), 222105.

(4) Neusel, L.; Bivour, M.; Hermle, M. Selectivity Issues of MoOx Based Hole Contacts. *Energy Procedia* **2017**, *124*, 425−434.

(5) Garland, B. M.; Davis, B. E.; Strandwitz, N. C. Investigating the Effect of Aluminum Oxide Fixed Charge on Schottky Barrier Height in Molybdenum Oxide-Based Selective Contacts. *Sol. Energy Mater. Sol. Cells* **2023**, *262*, 112537.

(6) Pulfrey, D. L.; McOuat, R. F. Schottky-Barrier Solar-Cell Calculations. *Appl. Phys. Lett.* **1974**, *24* (4), 167−169.

(7) Lam, Y. W. Min m.i.s. Schottky Barrier Solar Cells—a Review. *Radio Electron. Eng.* **1981**, *51* (9), 447−454.

(8) Sun, Y.; Kang, X.; Zheng, Y.; Lu, J.; Tian, X.; Wei, K.; Wu, H.; Wang, W.; Liu, X.; Zhang, G. Review of the Recent Progress on GaN-Based Vertical Power Schottky Barrier Diodes (SBDs). *Electronics* **2019**, *8* (5), 575.

(9) Schroder, D. K. *Semiconductor Material and Device Characterization*, 3rd ed.; John Wiley & Sons, Inc., 2006; Vol. *44*.

(10) Yeo, Y. C.; Ranade, P.; King, T. J.; Hu, C. Effects of high-/spl kappa/gate dielectric materials on metal and silicon gate work-functions. *IEEE Electron Device Lett.* **2002**, *23* (6), 342−344.

(11) Connelly, D.; Faulkner, C.; Clifton, P. A.; Grupp, D. E. Fermi-Level Depinning for Low-Barrier Schottky Source/Drain Transistors. *Appl. Phys. Lett.* **2006**, *88*, 012105.

(12) Hu, J.; Nainani, A.; Sun, Y.; Saraswat, K. C.; Philip Wong, H. S. Impact of Fixed Charge on Metal-Insulator-Semiconductor Barrier Height Reduction. *Appl. Phys. Lett.* **2011**, *99*, 252104.

(13) Marstell, R. J.; Pugliese, A.; Strandwitz, N. C. Absence of Evidence for Fixed Charge in Metal-Aluminum Oxide-Silicon Tunnel Diodes. *Phys. Status Solidi B* **2019**, *256*, 1800342.

(14) Garland, B. M.; Davis, B. E.; Strandwitz, N. C. Exploiting Fixed Charge to Control Schottky Barrier Height in SilAl2O3|MoOx- Based Tunnel Diodes. *2021 IEEE 48th Photovoltaic Specialists Conference*, 2021; pp 2439−2442..

(15) Yamamoto, Y.; Kita, K.; Kyuno, K.; Toriumi, A. Study of La-Induced Flat Band Voltage Shift in Metal/HfLaO x/SiO2/Si Capacitors. *Jpn. J. Appl. Phys., Part 1* **2007**, *46* (11R), 7251−7255.

(16) Iwamoto, K.; Kamimuta, Y.; Ogawa, A.; Watanabe, Y.; Migita, S.; Mizubayashi, W.; Morita, Y.; Takahashi, M.; Ota, H.; Nabatame, T.; Toriumi, A. Experimental Evidence for the Flatband Voltage Shift of High- k Metal-Oxide-Semiconductor Devices Due to the Dipole Formation at the High- KSi O2 Interface. *Appl. Phys. Lett.* **2008**, *92*, 132907.

(17) Kirsch, P. D.; Sivasubramani, P.; Huang, J.; Young, C. D.; Quevedo-Lopez, M. A.; Wen, H. C.; Alshareef, H.; Choi, K.; Park, C. S.; Freeman, K.; Hussain, M. M.; Bersuker, G.; Harris, H. R.; Majhi, P.; Choi, R.; Lysaght, P.; Lee, B. H.; Tseng, H. H.; Jammy, R.; Böscke, T. S.; Lichtenwalner, D. J.; Jur, J. S.; Kingon, A. I. Dipole Model Explaining High-k/Metal Gate Field Effect Transistor Threshold Voltage Tuning. *Appl. Phys. Lett.* **2008**, *92*, 092901.

(18) Coss, B. E.; Loh, W. Y.; Carlo Floresca, H.; Kim, M. J.; Majhi, P.; Wallace, R. M.; Kim, J.; Jammy, R. Dielectric Dipole Mitigated Schottky Barrier Height Tuning Using Atomic Layer Deposited Aluminum Oxide for Contact Resistance Reduction. *Appl. Phys. Lett.* **2011**, *99* (10), 102108.

(19) Kita, K.; Toriumi, A. Origin of Electric Dipoles Formed at High- k/SiO2interface. *Appl. Phys. Lett.* **2009**, *94* (13), 92−95.

(20) Fujimura, N.; Ohta, A.; Ikeda, M.; Makihara, K.; Miyazaki, S. Direct Evaluation of Electrical Dipole Moment and Oxygen Density Ratio at High-k Dielectrics/SiO2 Interface by X-Ray Photoelectron Spectroscopy Analysis. *Jpn. J. Appl. Phys.* **2018**, *57*, 04FB07.

(21) Lin, L.; Robertson, J. Atomic Mechanism of Electric Dipole Formed at High-K: SiO2 Interface. *J. Appl. Phys.* **2011**, *109* (9), 094502.

(22) Zhu, L. Q.; Barrett, N.; Jégou, P.; Martin, F.; Leroux, C.; Martinez, E.; Grampeix, H.; Renault, O.; Chabli, A. X-Ray Photoelectron Spectroscopy and Ultraviolet Photoelectron Spectroscopy Investigation of Al-Related Dipole at the HfO2/Si Interface. *J. Appl. Phys.* **2009**, *105*, 024102.

(23) Coss, B. E.; Sivasubramani, P.; Brennan, B.; Majhi, P.; Wallace, R. M.; Kim, J. Measurement of Schottky Barrier Height Tuning Using Dielectric Dipole Insertion Method at Metal-Semiconductor Interfaces by Photoelectron Spectroscopy and Electrical Characterization Techniques. *J. Vac. Sci. Technol., B: Nanotechnol. Microelectron.: Mater., Process., Meas., Phenom.* **2013**, *31* (2), 021202.

(24) Kern, W. The Evolution of Silicon Wafer Cleaning Technology. *J. Electrochem. Soc.* **1990**, *137* (6), 1887−1892.

(25) Gelderman, K.; Lee, L.; Donne, S. W. Flat-Band Potential of a Semiconductor: Using the Mott-Schottky Equation. *J. Chem. Educ.* **2007**, *84* (4), 685−688.

(26) Bhuiyan, A. S.; Martinez, A.; Esteve, D. A New Richardson Plot for Non-Ideal Schottky Diodes. *Thin Solid Films* **1988**, *161*, 93−100.

(27) Terman, L. M. An Investigation of Surface States at a Silicon/Silicon Oxide Interface Employing Metal-Oxide-Silicon Diodes. *Solid-State Electron.* **1962**, *5*, 285−299.

(28) Groner, M. D.; Fabreguette, F. H.; Elam, J. W.; George, S. M. Low-Temperature Al2O3 Atomic Layer Deposition. *Chem. Mater.* **2004**, *16* (4), 639−645.

(29) Lee, B. H.; Anderson, V. R.; George, S. M. Growth and Properties of Hafnicone and HfO2/Hafnicone Nanolaminate and Alloy Films Using Molecular Layer Deposition Techniques. *ACS Appl. Mater. Interfaces* **2014**, *6* (19), 16880−16887.

(30) Abendroth, B.; Moebus, T.; Rentrop, S.; Strohmeyer, R.; Vinnichenko, M.; Weling, T.; Stöcker, H.; Meyer, D. C. Atomic Layer Deposition of TiO2 from Tetrakis(Dimethylamino) Titanium and H2O. *Thin Solid Films* **2013**, *545*, 176−182.

(31) Vasudev, P. K.; Mattes, B. L.; Pietras, E.; Bube, R. H. Excess Capacitance and Non-Ideal Schottky Barriers on GaAs. *Solid-State Electron.* **1976**, *19*, 557−559.

(32) Tung, R. T. schottky barrier heights of single crystal silicides on si(111). *J. Vac. Sci. Technol., B: Microelectron. Nanometer Struct.—Process., Meas., Phenom.* **1984**, *2* (3), 465−470.
(33) Werner, J. H.; Güttler, H. H. Barrier Inhomogeneities at Schottky Contacts. *J. Appl. Phys.* **1991**, *69* (3), 1522−1533.
(34) Singhania, R. M.; Price, H.; Kounga, V. Y.; Davis, B.; Brüner, P.; Thorpe, R.; Hynek, D. J.; Cha, J. J.; Strandwitz, N. C. Surface Characterization of Ultrathin Atomic Layer Deposited Molybdenum Oxide Films Using High-Sensitivity Low-Energy Ion Scattering. *J. Vac. Sci. Technol., A* **2021**, *39* (6), 063210.
(35) *CRC Handbook of Chemistry and Physics*, 95th ed.; Haynes, W. M.; Lide, D. R.; Bruno, T. J., Eds.; CRC Press: Boca Raton, FL, 2014.
(36) Park, T. J.; Byun, Y. C.; Wallace, R. M.; Kim, J. Impurity and Silicate Formation Dependence on O3 Pulse Time and the Growth Temperature in Atomic-Layer-Deposited La2O3 Thin Films. *J. Chem. Phys.* **2017**, *146*, 052821.
(37) Davis, B. E.; Strandwitz, N. C. Atomic Layer Deposited Bilayers and the Influence on Metal-Insulator-Semiconductor Schottky Barriers. *2022 IEEE 49th Photovoltaics Specialists Conference*, 2022; pp 1323−1328..
(38) Zhou, Y.; Ogawa, M.; Han, X.; Wang, K. L. Alleviation of Fermi-Level Pinning Effect on Metal/Germanium Interface by Insertion of an Ultrathin Aluminum Oxide. *Appl. Phys. Lett.* **2008**, *93* (20), 91−94.
(39) Nishimura, T.; Kita, K.; Toriumi, A. A Significant Shift of Schottky Barrier Heights at Strongly Pinned Metal/Germanium Interface by Inserting an Ultra-Thin Insulating Film. *Appl. Phys. Express* **2008**, *1*, 051406.
(40) Zhou, Y.; Han, W.; Wang, Y.; Xiu, F.; Zou, J.; Kawakami, R. K.; Wang, K. L. Investigating the Origin of Fermi Level Pinning in Ge Schottky Junctions Using Epitaxially Grown Ultrathin MgO Films. *Appl. Phys. Lett.* **2010**, *96*, 102103.
(41) Rangan, S.; Bersch, E.; Bartynski, R. A.; Garfunkel, E.; Vescovo, E. Band Offsets of a Ruthenium Gate on Ultrathin High- κ Oxide Films Phys. Rev. B: Condens. Matter Mater. Phys.on Silicon. *Phys. Rev. B - Condens. Matter Mater. Phys.* **2009**, *79*, 075106.
(42) Yin, X.; Battaglia, C.; Lin, Y.; Chen, K.; Hettick, M.; Zheng, M.; Chen, C.; Kiriya, D.; Javey, A. 19.2% Efficient InP Heterojunction Solar Cell with Electron-Selective TiO2 Contact. *ACS Photonics* **2014**, *1*, 1245−1250.
(43) Tsou, K. Y.; Hensley, E. B. Electron Affinities of the Alkaline Earth Chalcogenides. *J. Appl. Phys.* **1974**, *45* (1), 47−49.
(44) Kadir, R. A.; Rani, R. A.; Zoolfakar, A. S.; Ou, J. Z.; Shafiei, M.; Wlodarski, W.; Kalantar-Zadeh, K. Nb2O5 Schottky Based Ethanol Vapour Sensors: Effect of Metallic Catalysts. *Sens. Actuators, B* **2014**, *202*, 74−82.
(45) Filho, L. F.; Pansini, F. N. N.; de Souza, F. A. L. Size and shape effects on the stability, electronic structure, and Raman spectroscopy of $(SrO)_n$ nanoclusters. *Int. J. Quantum Chem.* **2021**, *121* (12), No. e26642.
(46) Kandpal, K.; Gupta, N. Investigations on High-κ Dielectrics for Low Threshold Voltage and Low Leakage Zinc Oxide Thin-Film Transistor, Using Material Selection Methodologies. *J. Mater. Sci.: Mater. Electron.* **2016**, *27* (6), 5972−5981.
(47) Filatova, E. O.; Konashuk, A. S. Interpretation of the Changing the Band Gap of Al2O3 Depending on Its Crystalline Form: Connection with Different Local Symmetries. *J. Phys. Chem. C* **2015**, *119* (35), 20755−20761.
(48) Alimardani, N.; King, S. W.; French, B. L.; Tan, C.; Lampert, B. P.; Conley, J. F. Investigation of the Impact of Insulator Material on the Performance of Dissimilar Electrode Metal-Insulator-Metal Diodes. *J. Appl. Phys.* **2014**, *116*, 024508.
(49) Kim, G. M.; Lee, S. M.; Michler, G. H.; Roggendorf, H.; Gösele, U.; Knez, M. Nanostructured Pure Anatase Titania Tubes Replicated from Electrospun Polymer Fiber Templates by Atomic Layer Deposition. *Chem. Mater.* **2008**, *20* (9), 3085−3091.
(50) Park, C.; Lee, C.; Lee, W.; Lee, J.; Kim, J.; Eom, D.; Oh, J.; Lee, S. H.; Kim, H. Thermal Stability of MgO Film on Si Grown by Atomic Layer Deposition Using Mg(EtCp)2 and H2O. *Ceram. Int.* **2021**, *47* (22), 31583−31589.
(51) Hou, X. Y.; Tan, J.; Hu, C. E.; Chen, X. R.; Geng, H. Y. Thermoelectric Properties of Strontium Oxide under Pressure: First-Principles Study. *Phys. Lett. A* **2021**, *390*, 127083.
(52) Wang, X.; Liu, H.; Zhao, L.; Fei, C.; Feng, X.; Chen, S.; Wang, Y. Structural Properties Characterized by the Film Thickness and Annealing Temperature for La2O3 Films Grown by Atomic Layer Deposition. *Nanoscale Res. Lett.* **2017**, *12* (1), 233.
(53) Hu, J.; Saraswat, K. C.; Wong, H. S. Metal/III-V Schottky barrier height tuning for the design of nonalloyed III-V field-effect transistor source/drain contacts. *J. Appl. Phys.* **2010**, *107*, 063712.

https://doi.org/10.1021/acsaelm.3c01231
ACS Appl. Electron. Mater. 2024, 6, 770−776